The American Journal of Pathology, Vol. 178, No. 6, June 2011

DOI: 10.1016/j.ajpath.2011.02.014

Mouse Vein Graft Hemodynamic Manipulations to Enhance Experimental Utility

Peng Yu,*† Binh T. Nguyen,* Ming Tao,* Yingnan Bai,‡ and C. Keith Ozaki*

From the Division of Vascular and Endovascular Surgery, Brigham and Women's Hospital, Harvard Medical School, Boston, Massachusetts; and the Departments of Vascular Surgery,† and Cardiology,‡ Zhongshan Hospital, Fudan University, Shanghai, China*

Mouse models serve as a tool to study vein graft failure. However, in wild-type mice, there is limited intimal hyperplasia, hampering efforts to identify anti–intimal hyperplasia therapies. Furthermore, vein graft wall remodeling has not been well quantified in mice. We hypothesized that simple hemodynamic manipulations can reproducibly augment intimal hyperplasia and remodeling end points in mouse vein grafts, thereby enhancing their experimental utility. Mouse inferior vena cava–to-carotid interposition isografts were completed using an anastomotic cuff technique. Three flow restriction manipulations were executed by ligating outflow carotid branches, creating an outflow common carotid stenosis, and constructing a midgraft stenosis. Flowmetry and ultrasonography were used perioperatively and at day 28. All ligation strategies decreased the graft flow rate and wall shear stress. Morphometry showed that intimal thickness increased by 26% via carotid branch ligation and by 80% via common carotid stenosis. Despite similar mean flow rates and shear stresses among the three manipulations, the flow waveform amplitudes were lowest with common carotid stenosis. The disordered flow of the midgraft stenosis yielded poststenotic dilatation. The creation of an outflow common carotid stenosis generates clinically relevant (poor runoff) vein graft low wall shear stress and offers a technically flexible method for enhancing the intimal hyperplasia response. Midgraft stenosis exhibits poststenotic positive wall remodeling. These reproducible approaches offer novel strategies for increasing the utility of mouse vein graft models. ***(Am J Pathol 2011, 178:2910–2919; DOI: 10.1016/j.ajpath.2011.02.014)***

Mouse vein graft models serve as a practical research tool to study intimal hyperplasia and wall remodeling of vein bypass graft and transplant failure, with several variations having been reported in the past decade.[1–5] Owing to relatively lower technical demand and its reduced bleeding, thrombosis, and mortality rates (and, consequently, high reproducibility), the cuff technique is widely used.[6–11] Although atherosclerosis-prone (such as apolipoprotein E–deficient) mice show higher intimal and wall thickening,[6,12] approximately 23% of human vein graft failure still occurs without presenting hyperlipidemia.[13] Normolipidemia and hyperlipidemia clinical conditions have similar incidence rates of graft failure,[13] and there is a lack of direct evidence that hyperlipidemia is an independent risk factor for human vein graft failure.[14–17] Also, to avoid the complicated atherosclerotic backgrounds, many mouse vein graft studies use wild-type (mostly C57BL/6 background) mice with a standard diet, which by the cuff and hand-sewn techniques at the common time points (postoperatively 4 weeks, 6 weeks, or even 6 months) does not show substantial intimal and wall adaptations that simulate human vein graft failure.[18] The mild intimal hyperplasia decrement from vein graft antifailure therapies may be obscured by some difficult-to-control factors (such as variations in surgical and fixation manipulations) and, consequently, may hamper efforts to statistically identify these therapeutic strategies to attenuate intimal hyperplasia and negative wall remodeling.

Experimental hemodynamic manipulation of blood vessels to dissect mechanisms of wall adaptations stands as a recognized research strategy,[19,20] and this approach has also been adopted for vein grafts.[11,21–24] We hypothesized that the modification of mouse vein graft hemodynamics can not only yield mechanistic information on the interplay between biomechanical forces and vascular adaptations but also increase their rele-

Supported by grants from the National Heart, Lung, and Blood Institute (R01HL079135 and T32HL007734) and the Carl and Ruth Shapiro Family Foundation.

Accepted for publication February 10, 2011.

None of the authors disclosed any relevant financial relationships.

Address reprint requests to C. Keith Ozaki, M.D., Division of Vascular and Endovascular Surgery, Brigham and Women's Hospital, 75 Francis St., Boston, MA 02115. E-mail: ckozaki@partners.org.

vance to the human conditions and augment various desired experimental end points (intimal hyperplasia, wall remodeling, etc). To test this hypothesis, we reconstructed the cuff technique mouse vein graft model with three different novel flow restriction manipulations and completed parallel hemodynamic, ultrasonographic, and detailed morphologic analyses.

Materials and Methods

Mice

Nine-week-old male C57BL/6J mice weighing 20 to 24 g were purchased from The Jackson Laboratory (Bar Harbor, ME). The animals were maintained on a 12-hour light/dark cycle, and they received water and standard chow ad libitum. All animal experiments were performed according to protocols approved by the Institutional Animal Care and Use Committee and complied with the *Guide for the Care and Use of Laboratory Animals*.[25]

Mouse Vein Graft Models Under Various Flow Situations

All operative procedures were performed aseptically, with general continuous isoflurane inhalant anesthesia (1% to 2% isoflurane mixed with 1 L/min oxygen), using a Zeiss binocular OPMI MD surgical microscope (zoom, ×4 to ×24; Carl Zeiss Inc., Oberkochen, Germany) connected to a Canon EOS Rebel T1i SLR camera (Canon Inc., Lake Success, NY) via an ACCU-Beam adaptor (TTI Medical, San Ramon, CA) for micrography.

Mouse vein bypass isograft was generated via interposition of a supradiaphragmatic inferior vena cava from a donor mouse into the right common carotid artery of a recipient mouse, similar to the report by Zou et al[1] with modifications. Briefly, the mouse right common carotid artery was mobilized free from surrounding connective tissues as far distally and proximally as possible. It was then ligated using 9−0 nylon sutures at the midpoint and divided. After clamping, the ligatures were removed, and the proximal and distal artery ends were everted over premade polyetheretherketone cuffs (Zeus Inc., Orangeburg, SC), which had a 0.51-mm outside diameter (OD), a 0.41-mm inside diameter, and an approximately 0.60-mm-long cuff body. The inferior vena cava was then sleeved over the cuffed arterial ends and was secured in position using another 9−0 suture.

Normal-flow mice (Figure 1A) had no further manipulations (n = 8). In additional mice, flow reduction was achieved through one of three constructions: outflow carotid artery branch ligation (n = 15), outflow common carotid artery focal stenosis (n = 11), or midgraft focal stenosis (n = 5).

Outflow restriction was generated by ligating the ipsilateral internal carotid artery plus the occipital artery (Figure 1B) or by gently placing a 9−0 ligature over the outflow common carotid artery (approximately 1 mm from the tail of the distal cuff body) using an external mandrel (33-gauge blunt needle; OD, 0.21 mm; Hamilton Co., Reno, NV) and then removing the needle to restore blood flow (Figure 1C). A midgraft focal stenosis was constructed by placing the ligature over the middle portion of the vein graft using a 32-gauge blunt needle (OD, 0.23 mm; Hamilton Co.) and then removing the needle (Figure 1D). High-resolution micrography was used during surgery and harvest to determine vein graft external dimensions.

Flowmetry

To monitor blood flow change among vein grafts, flow rate was measured before and more than 20 minutes after vein graft flow restriction (to avoid any possible vessel spasms) and before harvest (day 28) using a flow meter (model TS420) with a flow probe (model 1PRB; both from Transonic Systems Inc., Ithaca, NY) and a data acquisition system (PowerLab 4/30 with LabChart v7.0.2; ADInstruments Inc., Colorado Springs, CO). All the data were acquired under a consistent respiratory rate and from the middle portion of each vein graft (the middle portion of each half graft of the midgraft stenosis model).

Ultrasonography for Vein Graft Dimension Measurement

High-resolution ultrasonography of postoperative mouse vein grafts was completed at days 4 and 28 using a Vevo 2100 imaging system with 18- to 70-MHz linear array transducers (VisualSonics Inc., Toronto, ON, Canada). Mice were anesthetized with inhaled isoflurane, and body temperature was maintained using a 37°C heated stage. Depth of anesthesia, heart rate, and respirations were continuously monitored. Color and pulsed wave Doppler modes were used to evaluate flow turbulence, M-mode for vessel cross-sectional dimensions, and B-mode for vessel length.

Tissue Harvest and Processing

Vein grafts were collected at postoperative day 28 for morphometric analysis. Whole-body perfusion fixation (by 10% formalin) under physiologic mean arterial pressure (100 mmHg) was completed by intravascular access via the left ventricle. The vein graft segment was gently harvested, *in vitro* formalin fixed, processed, and paraffin embedded. Using the cuff edges and midgraft ligature (for the midgraft stenosis model) as landmarks, paraffin serial sections were obtained at 100- to 200-μm intervals.

As shown via horizontal planes in the schemata in Figure 1, the cross sections 400 and 600 μm from the proximal/distal cuff edge were selected to represent the proximal/distal vein graft. Similarly, the 400- and 600-μm cross sections proximal/distal to the stenosis site in the midgraft stenosis model also represented the proximal/distal midgraft. Masson's trichrome staining and computer image processing (Zeiss Axio A1 microscope and AxioCam HRc camera, with AxioVision Rel 4.7;

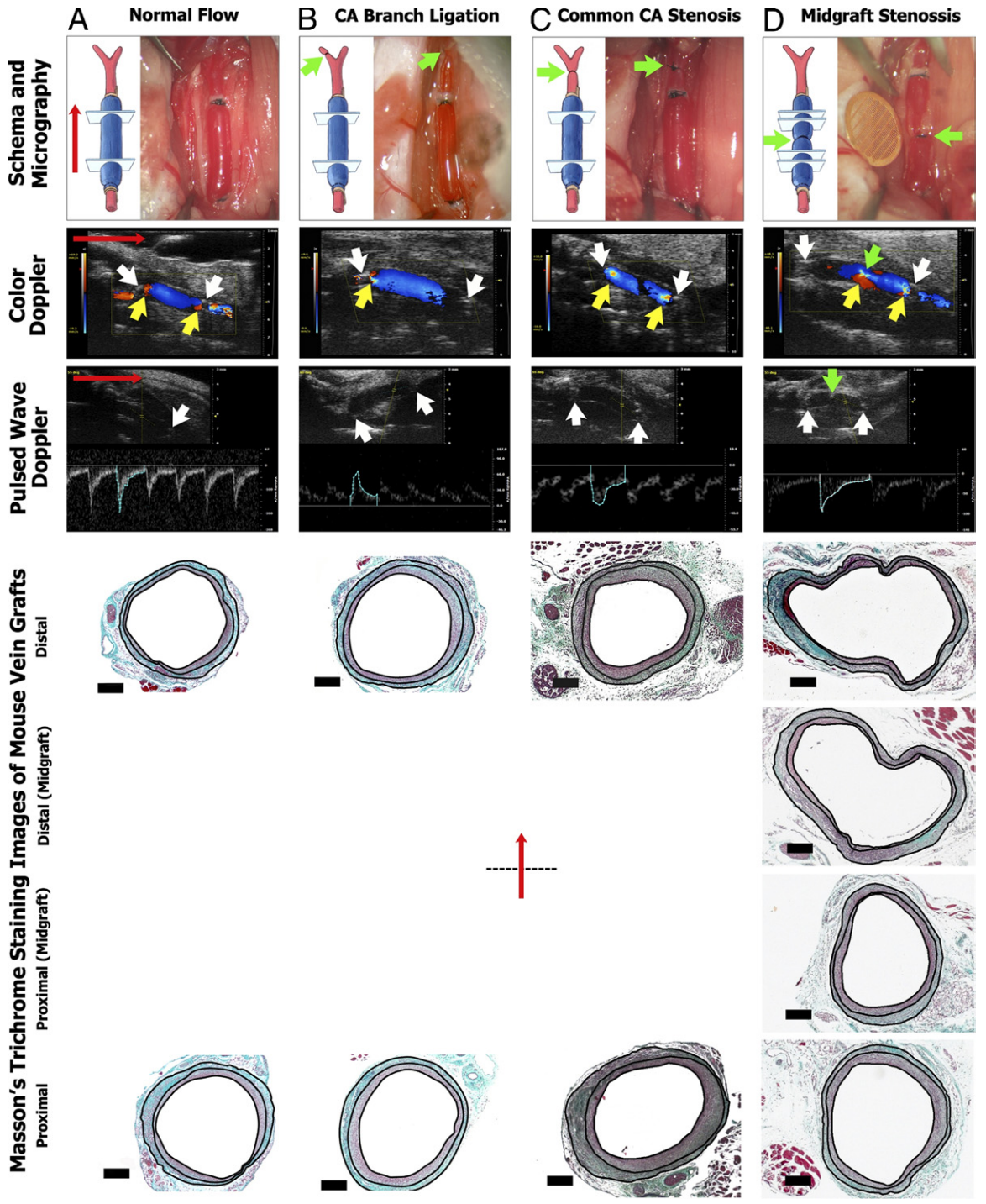

Figure 1. Hemodynamically modified cuff technique mouse vein graft models. **A:** Normal-flow model. **B:** Outflow carotid artery (CA) restriction by ligating the internal CA plus the occipital artery. **C:** Outflow common CA 33-gauge focal stenosis model. **D:** Midgraft 32-gauge focal stenosis model. The horizontal planes in the schemata show the locations of histologic sections for Masson's trichrome staining and morphologic analysis. Micrography was performed after each model was completed. An electron microscopy mesh was used in micrography for the midgraft stenosis model (**D**) for accurate vessel scaling. Representative color and pulsed wave Doppler sonograms of mouse vein grafts at day 4 are shown. Pulsed wave Doppler images were captured 900 μm from the distal cuff or midgraft ligature. **Red arrows** depict blood flow direction; **green arrows**, ligation sites; **white arrows**, cuffs; and **yellow arrows**, blood flow turbulence. The image colors represent the direction and magnitude of the Doppler signal frequency shift. Representative Masson's trichrome staining of the serial sections for that portion of the vein graft are shown. Red staining depicts cytoplasm and muscle fibers; green, collagen; and black, cell nuclei. Three black lines delineate the boundaries of different layers of vein graft wall (from the lumen to the outside): lumen boundary, internal elastic lamina, and outside boundary. Between the lumen boundary and the internal elastic lamina = intima; and between the internal elastic lamina and the outside boundary = M+A. Scale bars = 200 μm.

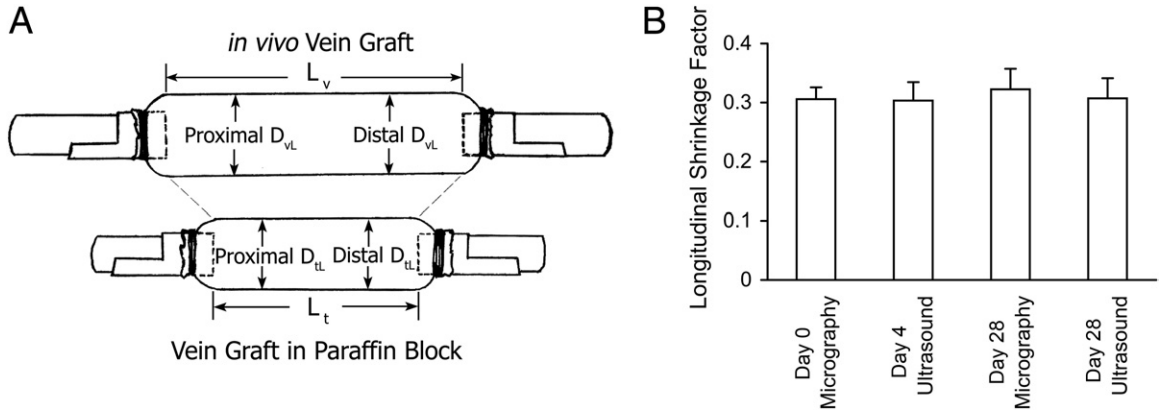

Figure 2. Vein graft shrinkage factor calculation. **A:** Schematic drawing of an *in vivo/in vitro* vein graft labeled with lengths and diameters. **B:** Vein graft SF_L results calculated by micrography (at days 0 and 28) and by B-mode ultrasonography (at days 4 and 28). Error bars represent SEM.

Carl Zeiss Inc.) were used. We used Masson's staining strategy as rationalized previously[18]: the continuous green lines in these sections correlate well with the elastic lamina fibers in Van Gieson's–stained murine vein graft sections.

Calculation of Vein Graft Shrinkage Factors

Due to the loss of longitudinal stretch from the common carotid artery on the two sides of the vein graft, shrinkage via tissue processing (fixation, dehydration, and paraffin cooling), and possible nonideal perfusion fixation (leading to elastic lamina recoil), the geometric characteristics of vein graft tissue in the paraffin block for final morphologic analysis may not reflect the *in vivo* situation. Thus, vein graft longitudinal shrinkage factor (SF_L) and cross-sectional shrinkage factor (SF_C) were determined.

Micrography [at day 0 after vein implantation and at day 28 before harvest, with a G7530-Cu rectangular mesh (Electron Microscopy Sciences, Hatfield, PA) for scaling, as shown in Figure 1D] and B-mode ultrasonography (at days 4 and 28) were used to measure *in vivo* vein graft length (L_v in Figure 2A). The length of the formalin-fixed, paraffin-embedded (FFPE) *in vitro* vein graft (L_t) was measured by counting serial sections. Thus, the formula for calculating the SF_L was as follows: $SF_L = (L_v - L_t)/L_v$. The results at different time points via micrography or ultrasonography were quite consistent (shown in Figure 2B), so we chose 0.31 as an SF_L constant value of our mouse vein graft models, which meant that the vein graft in paraffin block was on average 31% shorter longitudinally than its *in vivo* one, and 400- and 600-μm paraffin cross sections were approximately identical to the *in vivo* 600- and 900-μm relative locations to the landmark.

Based on the SF_L, the SF_C was calculated. Day 28 *in vivo* vein graft lumen diameter (D_{vL} in Figure 2A; localized at proximal and distal 900 μm) was measured using M-mode ultrasonography. *In vitro* vein graft (day 28) concentric lumen diameter (D_{tL}; not cross-sectional lumen diameter given that several of the thin grafts harvested failed to hold their cylindrical geometry during fixation and embedding; see the calculation in the *Morphometry of Masson's-Stained Sections* subsection) was from either the proximal or distal 600-μm section. An SF_C was calculated as follows: $SF_C = (D_{vL} - D_{tL})/D_{vL}$. The mean ± SEM result of the proximal SF_C was 0.16 ± 0.02 and of the distal SF_C was 0.14 ± 0.04.

Calculation of Vein Graft Wall Shear Stress

From Doppler scanning of these vein graft models, there was noticeable flow turbulence only near landmarks [approximately confined to the *in vivo* 300-μm zone close to the cuff and the 500-μm poststenotic zone of the midgraft stenosis model, as shown in Figure 1 (color Doppler)], and *in vivo* 600- to 900-μm locations rarely had obvious flow turbulence [Figure 1 (pulsed wave Doppler)]; thus, we assumed Poiseuille (laminar) flow and calculated vein graft mean wall shear stress as follows: $\tau = 32\mu Q/\pi D^3$, where Q is the mean flow rate; μ, the viscosity of blood (0.035 Poise); and D, the day 0 *in vivo* vein graft lumen diameter (D_{0vL}) or the day 28 *in vivo* lumen diameter (D_{vL}). D_{0vL} was calculated as follows from the deduction of two times the mean normal inferior vena cava wall thickness (approximately 12 μm; 100 mmHg; $n = 3$ in a separate experiment) from the OD of each day 0 *in vivo* vein graft (D_{0vO}): $D_{0vL} = D_{0vO} - 24$ μm. Based on the SF_C constant value calculated previously herein, the D_{vL} of each vein graft was estimated from its day 28 *in vitro* (histologic) concentric lumen diameter (D_{tL}) as follows: $D_{vL} = D_{tL}/(1 - SF_C)$.

Morphometry of Masson's-Stained Sections

The boundary of the lumen, the internal elastic lamina, and the outside boundary of the vein graft to adjunctive tissue were carefully recognized and traced as previously reported,[18] and, consequently, the circumferences and included areas of these three lines were obtained using AxioVision Rel 4.7 software (Carl Zeiss Inc.). Specifically, we identified the elastic lamina as internal elastic lamina by the α-actin expression (IMMH2-1KT; Sigma-Aldrich, St. Louis, MO; by the manufacturer's instructions) seen beyond it in the inferior vena cava and day 28 vein graft as previously described.[18] The media, adventitia,

and fibrous scar tissue are a continuum that physically and biologically constitutes the outer vein graft wall dense structure, thus we labeled them as M+A.[18] Several variables were calculated via the following formulas: concentric lumen diameter, $D_{tL} = C_L/\pi$; concentric lumen area, $A_{tL} = C_L^2/4\pi$; intimal thickness, $T_I = (A_I^{1/2} - A_L^{1/2})/\pi^{1/2}$; and M+A thickness, $T_{MA} = (A_O^{1/2} - A_I^{1/2})/\pi^{1/2}$, where C_L is the circumference of the lumen and A_L, A_I, and A_O are the cross-sectional inclusive areas of the lumen circumference, internal elastic lamina, and outside boundary, respectively. The "thickness," not "area," variables were selected because the latter may not be an accurate reflection of vein graft wall morphologic features if outward/inward wall remodeling took place.[18]

The remodeling index (RI) was calculated in a manner similar to previous reports.[26,27] The relation between vein graft wall area (A_W) and outside boundary including area (A_O; including wall area plus concentric lumen area) was evaluated by linear regression analysis: $A_O = aA_W + b$, where *a* (the regression coefficient or slope) is defined as RI and *b* is the intercept. Although the threshold of RI remains controversial, we adopted the criteria from arterial studies[27] and defined vein graft inward (negative) remodeling as RI < 0.75, outward (positive) remodeling as RI > 1.25, and compensatory remodeling as $0.75 \leq$ RI ≤ 1.25.

Statistical Analyses

Data are expressed as mean ± SEM. Statistical tests were completed using SigmaPlot v11.0 (Systat Software Inc., San Jose, CA) or Excel 2003 (Microsoft Corp., Redmond, WA). Comparison of two groups was performed using the unpaired two-tailed Student's *t*-test. Differences among more than two groups were analyzed by one-way analysis of variance.

Results

No mice died and there were no clinically apparent postoperative stroke symptoms in any experimental group. Two of 11 vein grafts in the outflow common carotid 33-gauge stenosis group were found to be occluded (with tremendous intimal hyperplasia) at harvest, although ultrasonography showed that they were patent at postoperative day 4. All other grafts were patent.

Blood Flowmetry

Although the cuff inside diameter may be slightly smaller than the average OD of *in vivo* mouse common carotid artery, no mean flow rate differences in the normal-flow group were found in ipsilateral native common carotid (at day 0 before vein implantation), vein graft (at days 0 and 28), and contralateral common carotid (at days 0 and 28) (data not shown). All flow restriction manipulations significantly decreased vein graft mean blood flow rates versus the baseline rate of each group at day 0 (approximately 50% decreased) and day 28 (mean ± SEM decrease: carotid branch ligation model, 66.23% ± 6.10%; common carotid stenosis model, 72.84% ± 4.29%; and midgraft stenosis model, 53.13% ± 3.13%). There were no differences in day 0 mean flow rate change among these three manipulations, but carotid branch ligation and outflow common carotid focal stenosis significantly exhibited a further decreased mean flow rate at harvest and the midgraft stenosis model showed little change (Figure 3A). All three flow manipulations decreased acute (day 0) and accommodated (day 28) mean wall shear stresses significantly (all >54% decreased), but there were no significant differences among the three manipulated models (Figure 3B).

In contrast, flow rate waveforms among the four vein graft models were quite different in morphologic features and regarding amplitude (Figure 4). All three flow restriction manipulations exhibited attenuated flow waveform amplitudes. Specifically, the two stenosis models acutely decreased their amplitudes at day 0, and the outflow common carotid stenosis situation showed progressive decrease until day 28. The difference in flow waveform amplitude between two outflow restriction models was consistently present: the outflow common carotid stenosis vein graft exhibited a significantly more attenuated waveform amplitude than did the carotid branch ligation model, with a lower peak value.

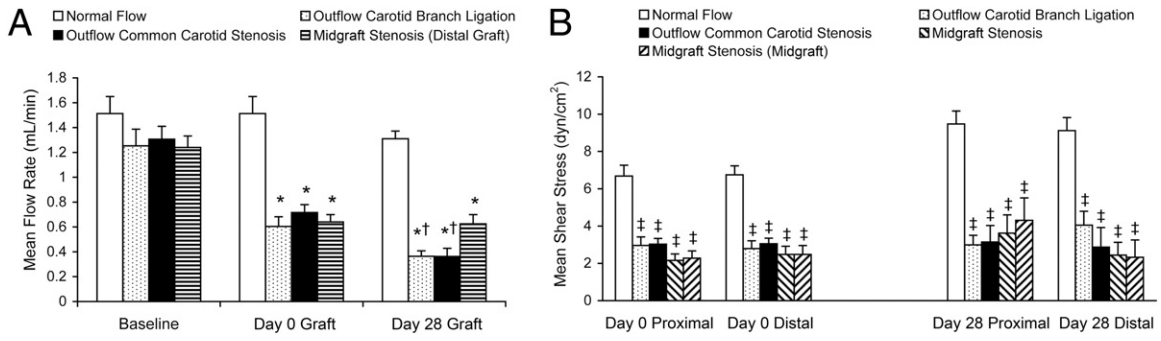

Figure 3. Flowmetry comparison of all four mouse vein graft models. **A:** Mean blood flow rate measured before (baseline) and after (day 0 graft) hemodynamic manipulation and at harvest (day 28 graft). **B:** Mean wall shear stress comparison: acute (day 0) shear stress calculated via micrography of *in vivo* vein grafts and day 28 shear stress calculated via adjusted *in vitro* histologic analysis. Values are shown as mean ± SEM (error bars). $^*P < 0.01$ versus baseline of each group; $^\dagger P < 0.05$ versus day 0 graft of each group; and $^\ddagger P < 0.01$ versus the normal-flow group at the same portion of vein graft.

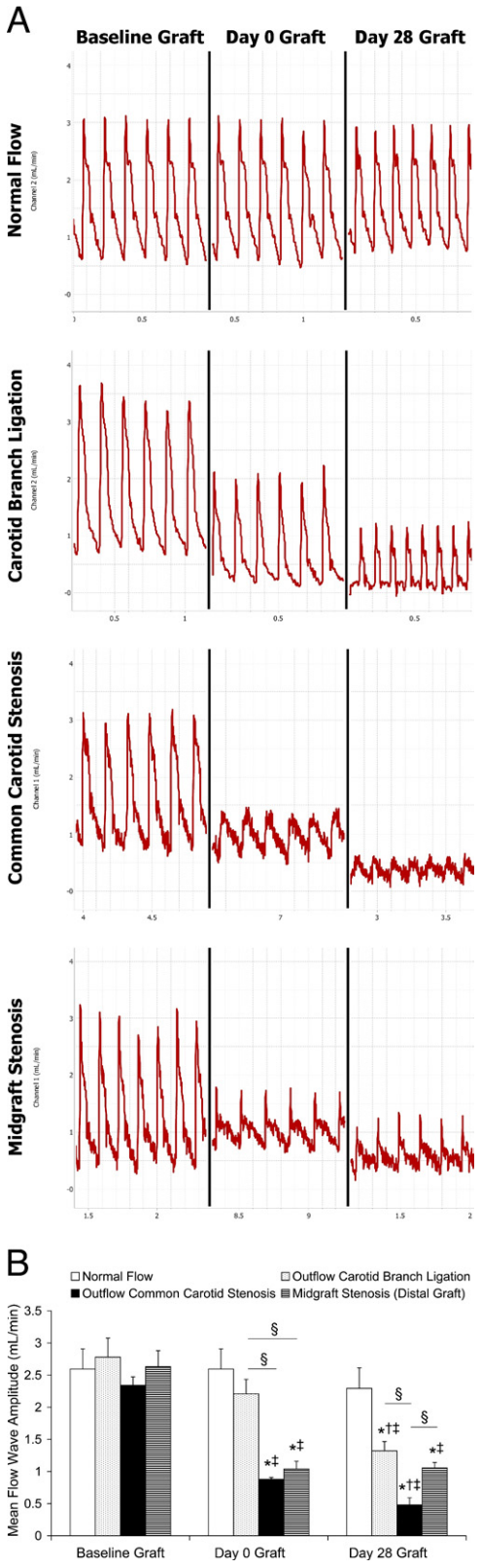

Figure 4. Vein graft blood flow rate waveforms. **A:** Representative waveforms of each group: baseline graft waveforms (before flow restriction), acute waveforms (day 0 graft after flow restriction; no restriction for the normal-flow group), and harvest waveforms (day 28). **B:** Comparisons of mean flow waveform amplitudes. Values are shown as mean ± SEM (error bars). $^{*}P < 0.01$ versus baseline of each group; $^{\dagger}P < 0.01$ versus day 0 graft of each group; $^{\ddagger}P < 0.05$ versus the normal-flow group at the same time point; and $^{\S}P < 0.05$.

Morphologic Analysis of Vein Graft Wall Adaptations

All relative flow uniform vein graft models (normal flow, outflow branch ligation, and outflow common carotid stenosis) showed a tendency toward the highest intimal hyperplasia at the proximal portion of the vein graft, the lowest in the middle portion, and intermediate at the distal portion. Normal-flow vein grafts developed mild intimal thickening along the graft: mean ± SEM of 49.64 ± 4.71 μm at the proximal portion and 42.63 ± 3.41 μm at the distal portion [Figure 1 (Masson's trichrome stain) and Figure 5A]. Outflow carotid branch ligation grafts exhibited moderately increased intimal hyperplasia [on average, 26.21% increased at the proximal portion ($P = 0.06$) and 38.36% at the distal portion ($P < 0.05$)]. The outflow common carotid 33-gauge focal stenosis model showed the highest intimal hyperplasia among the four groups: 79.15% increased at the proximal portion and 81.75% at the distal portion (both $P < 0.05$). The 32-gauge mandrel (OD, 0.23 mm) gave the midgraft stenosis model an approximately 78% reduction in lumen diameter (compared with the day 0 normal-flow vein graft *in vivo* mean lumen diameter of 1.04 mm via micrography), an approximately 50% mean flow rate decrease, and a >54% decrease in mean wall shear stress in both halves of the graft, whereas only the proximal half showed intermediate (56.98%) augmentation in mean intimal thickness. Meanwhile, the outflow common carotid stenosis and midgraft stenosis models mildly increased mean M+A thickness (Figure 5B).

To date, there are limited studies of vein graft wall remodeling (especially in mice) and few widely recognized morphologic variables to describe this pathologic change. We adopted three commonly used end points in arterial studies, intima/(M+A) thickness ratio, concentric lumen area, and RI, to describe wall remodeling after vein graft implantation.

Of the three flow manipulations, the midgraft stenosis procedure yielded significant changes in these remodeling variables [Figure 1 (Masson's trichrome stain)]. Specifically, the distal half of the vein graft of this model showed a significantly smaller intima/(M+A) thickness ratio (Figure 5C), a >56% larger concentric lumen area than all the other groups at the distal vein graft portion (Figure 5D), and outward vein graft wall remodeling (RI > 1.35), which especially presented at the distal midgraft portion (RI = 3.16; Figure 5E).

The vein graft deformation in the midgraft stenosis model led to differential flow turbulence and distinct morphologic patterns between the two halves; thus, the internal morphometric comparison between the proximal and distal counterparts was completed via serial sectioning and analyses. We found that only the distal 200- to 500-μm midgraft portion demonstrated significantly larger lumen radii, without obvious difference in intimal or wall thickness, suggesting localized and near pure poststenotic positive wall remodeling/dilatation (Figure 6).

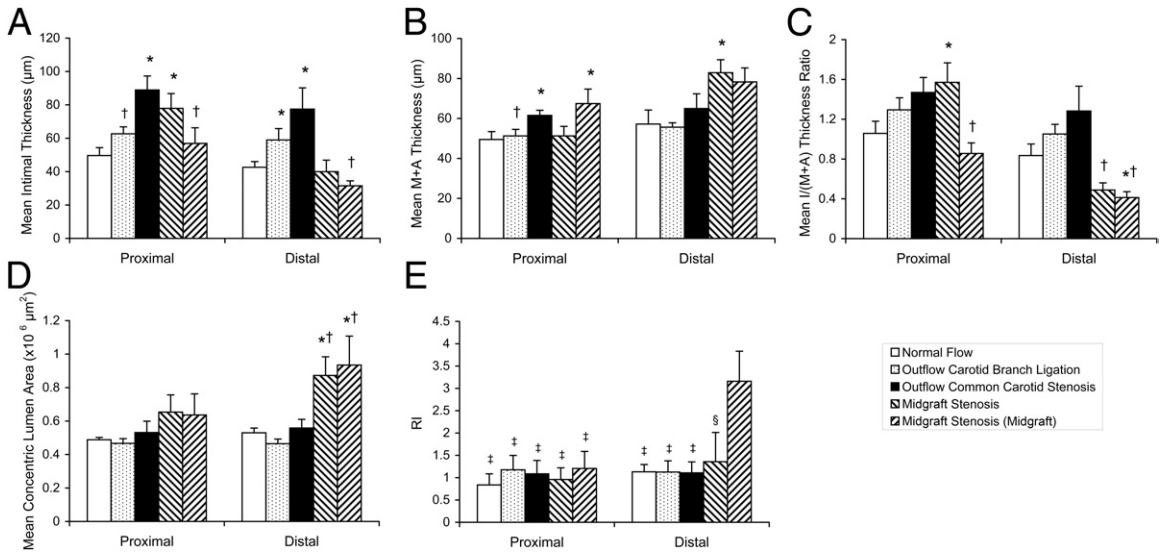

Figure 5. Morphologic analysis of mouse vein graft wall adaptation. The mean of any measurement from proximal/distal 400- and 600-μm sections or proximal/distal midgraft 400- and 600-μm sections (to the stenosis site) in the midgraft stenosis model are shown. **A:** Intimal thickness. **B:** M+A thickness. **C:** Intima (I)/(M+A) thickness ratio. **D:** Concentric lumen area. **E:** RI. Values are shown as mean ± SEM (error bars). $^{*}P < 0.05$ versus the normal-flow group at the same portion of vein graft; $^{\dagger}P < 0.05$ versus outflow 33-gauge common carotid stenosis group at the same portion of vein graft; $^{\ddagger}P < 0.05$; and $^{\S}P = 0.09$ versus the distal midgraft of the midgraft stenosis model.

Discussion

Herein we described a flexible focal stenosis strategy that reproducibly manipulated mouse vein graft hemodynamics, and these adjuncts resulted in defined alterations in vein graft morphologic features at day 28.

Owing to its relatively larger vessel dimension and subsequently lower microsurgical technical demands, the carotid artery is more widely used than is the femoral artery[3] for mouse vein graft studies. While the cerebral blood flow pattern differs from that in the peripheral circulation because of the relatively low resistance in the cerebral vascular bed[28] (which, consequently, has a higher flow rate[23,29] and higher mean wall shear stress[30]), one sees only moderate intimal hyperplasia in mouse carotid vein graft models, unsatisfactory for simulation of clinical bypass graft failure mechanisms. These murine grafts start with smooth muscle cells in the wall but no true neointima.[18] It has been previously reported that nonresident cells contribute to the subsequent neointima that develops with arterialization.[31,32]

Hemodynamic forces that affect intimal hyperplasia and wall adaptation have been described.[20,33–36] Re-

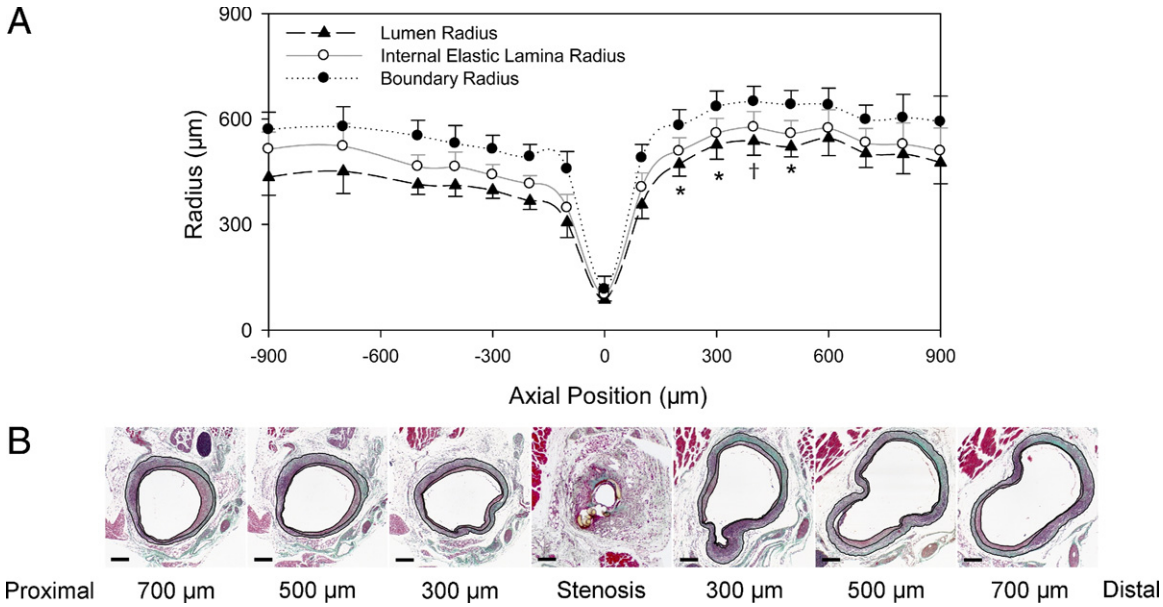

Figure 6. Morphologic analysis of the midgraft 32-gauge focal stenosis model. **A:** Radii of different vein graft layers corresponding to the axial position relative to the focal stenosis site. Values are shown as mean ± SEM (error bars). $^{*}P < 0.05$ and $^{\dagger}P = 0.051$ versus the counterpart at the proximal vein graft. **B:** Representative Masson's trichrome staining of the longitudinal serial cross sections. Scale bars = 200 μm.

searchers, therefore, used outflow artery branch ligation to decrease wall shear.[11,23] However, similar to what the outflow carotid branch (internal carotid plus occipital artery) ligation model showed here ligation of the external carotid artery only moderately enhanced the mouse intimal hyperplasia response.[18,23] Meanwhile, the less variable mouse carotid anatomy limits its ability to induce different levels of hemodynamic change to meet various experimental goals.[18]

Clinically, the vein graft patency rate is compromised in the setting of poor distal runoff (smaller size or diseased/narrowed) vessels,[37–40] and the outflow restriction manipulation probably better mimics this scenario over the low-resistance cerebral outflow. To extend this strategy to augment vein graft intimal or wall adaptations, we developed a novel outflow common carotid focal stenosis vein graft model. The 33-gauge external mandrel (OD, 0.21 mm) was selected to generate an approximately 50% (day 0) to approximately 75% (day 28) mean flow rate decrease, a >60% wall shear stress decrease, and, consequently, an 80% enhancement of intimal thickness. One main advantage of this external mandrel–induced focal stenosis strategy is its flexibility of application. As always, many determinants of the vein graft wall adaptations depend on the mouse strain and genetic background, diet type, surgical technique (including injury to the vascular wall, vein ischemia time based on the method of donor vein harvest either before or during recipient carotid operation, vein desiccation time, etc), cuff size, experiment duration, etc.[18] Researchers who want to use this novel strategy could select different mandrel sizes according to their research design needs and individual experimental conditions.

Whereas the values of traditional vascular hemodynamic variables (such as mean flow rates and mean wall shear stresses) were similar among all the flow restriction groups, subtle variations in the flow patterns were associated with the significant differentials in the final wall adaptations. This finding suggests a highly complex biomechanical environment in which shear stress is not the only major factor leading to intimal hyperplasia[41,42] and the mean value of wall shear stress is not enough to analyze the effect of hemodynamics on vascular wall adaptations. Pulsatility, flow amplitude, strain, and other biomechanical variables need to be characterized.

It is important to acknowledge that there is a complex interplay between biological and hemodynamic forces in vein graft adaptations: every severe vein graft narrowing derives from early mild to moderate lesions, and these early adaptations affect local hemodynamics, which subsequently contribute to the final vein graft wall adaptation/failure. The midgraft stenosis vein graft model was developed to investigate the impact of focal lumen narrowing on local hemodynamic forces and subsequent vein graft biological end points.

This midgraft 78% stenosis model developed approximately 57% more intimal hyperplasia than the normal-flow model at the proximal portion, although not as much as the reported 50% focal stenosis rabbit vein graft model.[43] Possible explanations are differences in local hemodynamic characteristics and species effects. With the midgraft focal stenosis (especially at the poststenotic 200- to 500-μm zone), positive vein graft wall remodeling took place (RI = 3.16, and the concentric lumen area was much larger) with modest intimal hyperplasia. Exacerbated flow turbulence at this zone may serve as an important contributor. These situations can simulate clinical vein graft poststenotic dilatation and positive remodeling presentations (Figure 7).[44,45] To our knowledge, no good vein graft wall remodeling animal models have been re-

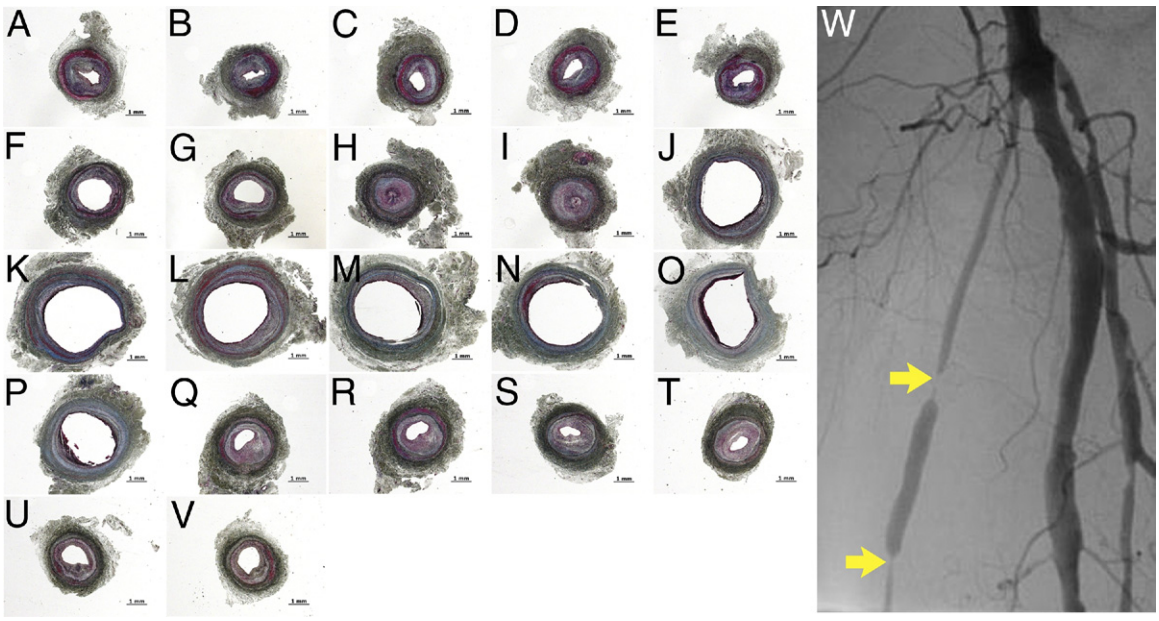

Figure 7. Intimal hyperplasia and wall remodeling took place in a failed 8-month-old human vein graft (originally from a uniform-sized anterior branch of the saphenous vein). **A–V:** Masson's trichrome staining of longitudinal serial (5-mm interval) cross sections. Intimal hyperplasia (all **A–V** images) and wall remodeling [negative remodeling, **A–I** (RI = 0.63); positive remodeling, **J–P** (RI = 1.28); and compensatory remodeling, **Q–V** (RI = 0.86)] can be found. Scale bars = 1 mm. **W:** Angiogram of the failing graft. **Yellow arrows** depict two stenosis sites.

ported to date. Although this midgraft stenosis mouse model holds some disadvantages (eg, more flow turbulence; poststenotic remodeling that is localized and uneven so that meticulous sectioning is needed), it may be used to study vein graft wall remodeling.

Finally, leveraging micrography and ultrasonography, we compared the *in vivo* anatomy with the *in vitro* histologic (10% FFPE) vein graft dimensions and introduced a new concept: longitudinal and cross-sectional shrinkage factors for these vascular tissues. Use of other tissue fixation strategies (eg, paraformaldehyde or glutaraldehyde) may alter the level of tissue shrinkage. These observations should be considered when researchers derive *in vivo* conclusions from histologic findings.

Limitations

This article focuses on the potential of these models, but several limitations are acknowledged. Day 28 is the most widely used time point in animal vein graft studies, and we are unable to provide insights into other time points. However, this work provides a standardized platform for future studies that might include additional time points while simultaneously drilling down on mechanisms linking the interplay of physical forces and vascular wall biology. We purposely interrogated portions of the conduit that have more laminar flow, but information on the impact of disordered flow (particularly with in the 500-μm poststenotic portion of the midgraft stenosis model) on these systems remains to be determined. Pressure analyses are not included in these experiments owing to the technical challenge of getting accurate pressure measurements in these small blood vessels. Owing to the difficulty in surgically exposing the mouse proximal common carotid artery, this external mandrel focal stenosis strategy may not be feasible to study impaired inflow situations. Finally, although the blood flow waveform amplitude correlation with final vascular morphologic features is novel, further research is required to delineate the precise biological mechanisms of this observation. This work focused on physical forces that can be manipulated to alter the wall adaptations. The standardized tools herein described can now be used to explore this complex interplay with biological mediators, especially because a murine platform is used.

Conclusions

A focal stenosis approach via an external mandrel technique offers a flexible strategy to broaden the experimental utility of mouse vein graft models. Surgical creation of an outflow common carotid stenosis generates clinically relevant (poor runoff) vein graft low wall shear stress, enhancing the intimal hyperplasia response of mouse vein grafts. Subtle variations in the conduit flow patterns result in significant differentials in the final wall adaptations, with low flow waveform amplitude being associated with accelerated vein graft wall adaptation. The midgraft focal stenosis model predominantly exhibits positive vein graft wall remodeling at the poststenotic portion. These approaches, especially when combined with genetic and dietary manipulations in mice, offer powerful tools for dissecting the mechanisms of vein graft failure.

Acknowledgments

We thank Christina Campagna, B.S. (Touro College of Osteopathic Medicine, New York, NY), for assisting with completion of the analyses and Christopher D. Owens, M.D. (University of California at San Francisco, San Francisco, CA), for providing human vein graft tissue blocks.

References

1. Zou Y, Dietrich H, Hu Y, Metzler B, Wick G, Xu Q: Mouse model of venous bypass graft arteriosclerosis. Am J Pathol 1998, 153:1301–1310
2. Zhang L, Hagen PO, Kisslo J, Peppel K, Freedman NJ: Neointimal hyperplasia rapidly reaches steady state in a novel murine vein graft model. J Vasc Surg 2002, 36:824–832
3. Cooley BC: Murine model of neointimal formation and stenosis in vein grafts. Arterioscler Thromb Vasc Biol 2004, 24:1180–1185
4. Diao Y, Xue J, Segal MS: A novel mouse model of autologous venous graft intimal hyperplasia. J Surg Res 2005, 126:106–113
5. Salzberg SP, Filsoufi F, Anyanwu A, von Harbou K, Karlof E, Carpentier A, Dansky HM, Adams DH: Increased neointimal formation after surgical vein grafting in a murine model of type 2 diabetes. Circulation 2006, 114:I302–I307
6. Lardenoye JH, de Vries MR, Lowik CW, Xu Q, Dhore CR, Cleutjens JP, van Hinsbergh VW, van Bockel JH, Quax PH: Accelerated atherosclerosis and calcification in vein grafts: a study in APOE*3 Leiden transgenic mice. Circ Res 2002, 91:577–584
7. Li X, Chyu KY, Faria Neto JR, Yano J, Nathwani N, Ferreira C, Dimayuga PC, Cercek B, Kaul S, Shah PK: Differential effects of apolipoprotein A-I-mimetic peptide on evolving and established atherosclerosis in apolipoprotein E-null mice. Circulation 2004, 110:1701–1705
8. Fogelstrand P, Osterberg K, Mattsson E: Reduced neointima in vein grafts following a blockage of cell recruitment from the vein and the surrounding tissue. Cardiovasc Res 2005, 67:326–332
9. Sedding DG, Hermsen J, Seay U, Eickelberg O, Kummer W, Schwencke C, Strasser RH, Tillmanns H, Braun-Dullaeus RC: Caveolin-1 facilitates mechanosensitive protein kinase B (Akt) signaling in vitro and in vivo. Circ Res 2005, 96:635–642
10. Cheng J, Du J: Mechanical stretch simulates proliferation of venous smooth muscle cells through activation of the insulin-like growth factor-1 receptor. Arterioscler Thromb Vasc Biol 2007, 27:1744–1751
11. Jiang Z, Yu P, Tao M, Ifantides C, Ozaki CK, Berceli SA: Interplay of CCR2 signaling and local shear force determines vein graft neointimal hyperplasia in vivo. FEBS Lett 2009, 583:3536–3540
12. Dietrich H, Hu Y, Zou Y, Huemer U, Metzler B, Li C, Mayr M, Xu Q: Rapid development of vein graft atheroma in ApoE-deficient mice. Am J Pathol 2000, 157:659–669
13. Alexander JH, Hafley G, Harrington RA, Peterson ED, Ferguson TB Jr., Lorenz TJ, Goyal A, Gibson M, Mack MJ, Gennevois D, Califf RM, Kouchoukos NT: Efficacy and safety of edifoligide, an E2F transcription factor decoy, for prevention of vein graft failure following coronary artery bypass graft surgery: PREVENT IV: a randomized controlled trial. JAMA 2005, 294:2446–2454
14. Abbruzzese TA, Havens J, Belkin M, Donaldson MC, Whittemore AD, Liao JK, Conte MS: Statin therapy is associated with improved patency of autogenous infrainguinal bypass grafts. J Vasc Surg 2004, 39:1178–1185
15. Conte MS, Bandyk DF, Clowes AW, Moneta GL, Namini H, Seely L: Risk factors, medical therapies and perioperative events in limb salvage surgery: observations from the PREVENT III multicenter trial. J Vasc Surg 2005, 42:456–465
16. Schanzer A, Hevelone N, Owens CD, Beckman JA, Belkin M, Conte MS: Statins are independently associated with reduced mortality in

patients undergoing infrainguinal bypass graft surgery for critical limb ischemia. J Vasc Surg 2008, 47:774–781
17. Monahan TS, Owens CD: Risk factors for lower-extremity vein graft failure. Semin Vasc Surg 2009, 22:216–226
18. Yu P, Nguyen BT, Tao M, Campagna C, Ozaki CK: Rationale and practical techniques for mouse models of early vein graft adaptations. J Vasc Surg 2010, 52:444–452
19. Kumar A, Lindner V: Remodeling with neointima formation in the mouse carotid artery after cessation of blood flow. Arterioscler Thromb Vasc Biol 1997, 17:2238–2244
20. Korshunov VA, Berk BC: Flow-induced vascular remodeling in the mouse: a model for carotid intima-media thickening. Arterioscler Thromb Vasc Biol 2003, 23:2185–2191
21. Morinaga K, Okadome K, Kuroki M, Miyazaki T, Muto Y, Inokuchi K: Effect of wall shear stress on intimal thickening of arterially transplanted autogenous veins in dogs. J Vasc Surg 1985, 2:430–433
22. Jiang Z, Berceli SA, Pfahnl CL, Wu L, Goldman D, Tao M, Kagayama M, Matsukawa A, Ozaki CK: Wall shear modulation of cytokines in early vein grafts. J Vasc Surg 2004, 40:345–350
23. Osterberg K, Mattsson E: Intimal hyperplasia in mouse vein grafts is regulated by flow. J Vasc Res 2005, 42:13–20
24. Jiang Z, Yu P, Tao M, Fernandez C, Ifantides C, Moloye O, Schultz GS, Ozaki CK, Berceli SA: TGF-β- and CTGF-mediated fibroblast recruitment influences early outward vein graft remodeling. Am J Physiol Heart Circ Physiol 2007, 293:H482–H488
25. National Institutes of Health: Guide for the Care and Use of Laboratory Animals. Bethesda, MD, National Institutes of Health, 1996. NIH publication 85–23
26. Korshunov VA, Berk BC: Strain-dependent vascular remodeling: the "Glagov phenomenon" is genetically determined. Circulation 2004, 110:220–226
27. Feldman CL, Coskun AU, Yeghiazarians Y, Kinlay S, Wahle A, Olszewski ME, Rossen JD, Sonka M, Popma JJ, Orav J, Kuntz RE, Stone PH: Remodeling characteristics of minimally diseased coronary arteries are consistent along the length of the artery. Am J Cardiol 2006, 97:13–16
28. Lui K, Hellmann J, Sprigg A, Daneman A: Cerebral blood-flow velocity patterns in post-hemorrhagic ventricular dilation. Childs Nerv Syst 1990, 6:250–253
29. Cabou C, Cani PD, Campistron G, Knauf C, Mathieu C, Sartori C, Amar J, Scherrer U, Burcelin R: Central insulin regulates heart rate and arterial blood flow: an endothelial nitric oxide synthase-dependent mechanism altered during diabetes. Diabetes 2007, 56:2872–2877
30. Cheng C, Helderman F, Tempel D, Segers D, Hierck B, Poelmann R, van Tol A, Duncker DJ, Robbers-Visser D, Ursem NT, van Haperen R, Wentzel JJ, Gijsen F, van der Steen AF, de Crom R, Krams R: Large variations in absolute wall shear stress levels within one species and between species. Atherosclerosis 2007, 195:225–235
31. Xu Q, Zhang Z, Davison F, Hu Y: Circulating progenitor cells regenerate endothelium of vein graft atherosclerosis, which is diminished in ApoE-deficient mice. Circ Res 2003, 93:e76–e86
32. Diao Y, Guthrie S, Xia SL, Ouyang X, Zhang L, Xue J, Lee P, Grant M, Scott E, Segal MS: Long-term engraftment of bone marrow-derived cells in the intimal hyperplasia lesion of autologous vein grafts. Am J Pathol 2008, 172:839–848
33. Friedman MH, Bargeron CB, Deters OJ, Hutchins GM, Mark FF: Correlation between wall shear and intimal thickness at a coronary artery branch. Atherosclerosis 1987, 68:27–33
34. Greenwald SE, Berry CL: Improving vascular grafts: the importance of mechanical and haemodynamic properties. J Pathol 2000, 190: 292–299
35. Haruguchi H, Teraoka S: Intimal hyperplasia and hemodynamic factors in arterial bypass and arteriovenous grafts: a review. J Artif Organs 2003, 6:227–235
36. Cunningham KS, Gotlieb AI: The role of shear stress in the pathogenesis of atherosclerosis. Lab Invest 2005, 85:9–23
37. Mii S, Okadome K, Onohara T, Yamamura S, Sugimachi K: Intimal thickening and permeability of arterial autogenous vein graft in a canine poor-runoff model: transmission electron microscopic evidence. Surgery 1990, 108:81–89
38. Itoh H, Komori K, Funahashi S, Okadome K, Sugimachi K: Intimal hyperplasia of experimental autologous vein graft in hyperlipidemic rabbits with poor distal runoff. Atherosclerosis 1994, 110:259–270
39. Seeger JM, Pretus HA, Carlton LC, Flynn TC, Ozaki CK, Huber TS: Potential predictors of outcome in patients with tissue loss who undergo infrainguinal vein bypass grafting. J Vasc Surg 1999, 30:427–435
40. Conte MS: Technical factors in lower-extremity vein bypass surgery: how can we improve outcomes? Semin Vasc Surg 2009, 22:227–233
41. Joshi AK, Leask RL, Myers JG, Ojha M, Butany J, Ethier CR: Intimal thickness is not associated with wall shear stress patterns in the human right coronary artery. Arterioscler Thromb Vasc Biol 2004, 24:2408–2413
42. Tran-Son-Tay R, Hwang M, Garbey M, Jiang Z, Ozaki CK, Berceli SA: An experiment-based model of vein graft remodeling induced by shear stress. Ann Biomed Eng 2008, 36:1083–1091
43. Meyerson SL, Refai D, Skelly CL, Curi MA, Glagov S, Schwartz LB: Hemodynamically "insignificant" stenoses stimulate neointimal thickening in experimental vein grafts. Int J Angiol 2001, 10:1061–1711
44. Cassina PC, Hailemariam S, Schmid RA, Hauser M: Infrainguinal aneurysm formation in arterialized autologous saphenous vein grafts. J Vasc Surg 1998, 28:944–948
45. Hong MK, Mintz GS, Hong MK, Abizaid AS, Pichard AD, Satler LF, Kent KM, Leon MB: Intravascular ultrasound assessment of the presence of vascular remodeling in diseased human saphenous vein bypass grafts. Am J Cardiol 1999, 84:992–998